



Effect of pyrolysis on microstructures made of various photoresists by two-photon polymerization: comparative study

M. I. SHARIPOVA,^{1,*}  T. G. BALUYAN,¹ K. A. ABRASHITOVA,¹ 
G. E. KULAGIN,¹ A. K. PETROV,¹ A. S. CHIZHOV,^{1,2}
T. B. SHATALOVA,² D. CHUBICH,³ D. A. KOLYMAGIN,³
A. G. VITUKHNOVSKY,^{3,4} V. O. BESSONOV,^{1,5}
AND A. A. FEDYANIN¹ 

¹Faculty of Physics, Lomonosov Moscow State University, Moscow 119991, Russia

²Faculty of Chemistry, Lomonosov Moscow State University, Moscow 119991, Russia

³Moscow Institute of Physics and Technology (National Research University), Moscow Region, Dolgoprudny 141700, Russia

⁴Lebedev Physical Institute, Russian Academy of Sciences, Moscow 119991, Russia

⁵Frumkin Institute of Physical Chemistry and Electrochemistry, Russian Academy of Sciences, Moscow 119071, Russia

*sharipova@nanolab.phys.msu.ru

Abstract: Two-photon laser polymerization (TPP) is a state-of-the-art technology that allows for the submicron-resolution printing of freeform 3D objects to be harnessed in various applications, including physics, biology, medicine, and materials science. The TPP is based on using photosensitive polymeric materials that impose restrictions on the minimum feature size and limit the functionality of printed structures within the capabilities of polymers. One of the promising yet insufficiently studied methods for overcoming these limitations is pyrolysis–high-temperature annealing of polymer objects in an inert atmosphere. It may allow both to decrease the size of the objects and modify their chemical composition. Here, we compare the effect of pyrolysis on solid objects being tens of micrometers in size printed by TPP from three commercially available photoresists: IP-Dip, OrmoComp, and SZ2080. For the annealing temperatures of 450°C and 690°C in an argon atmosphere, we assessed the changes in size, chemical composition, and adhesion to the silicon wafer substrate. Our data may be promising for developing pyrolysis as a standard post-processing method for structures created via TPP technology.

© 2021 Optical Society of America under the terms of the [OSA Open Access Publishing Agreement](#)

1. Introduction

Two-photon polymerization (TPP), or direct laser writing, proved to be a powerful tool to fabricate three-dimensional microstructures with a minimum feature size of down to 100 nm [1,2]. TPP enables microscale manufacturing of arbitrary 3D structures, including light-fueled automotive microwalkers [3], 3D invisibility optical cloaks [4], multi-lens objectives [5], free-form coupling elements [6], optical waveguides [7], microoptical elements [8], biocompatible microparticles [9], mechanical metamaterials [10], fiber-tip gas sensors [11], 3D cell scaffolds [12], and pH-driven micro-grippers [13]. One of the promising applications of TPP is producing of the refractive X-ray optical elements [14–16].

Despite some brilliant opportunities provided by TPP, its material selection is limited to polymer photoresists. Due to polymer transparency in the visible range, lack of electrical conductivity, mediocre mechanical properties, and low thermal and radiation stability, the practical application of TPP structures remains limited. For example, TPP-fabricated X-ray optics degrades after being exposed for several hours to intense X-ray radiation [16,17]. Moreover, material choice in

TPP defines a fundamental limit of resolution that can be achieved [18]. Conventional resolution of commercially available Nanoscribe GmbH Photonic Professional GT2 with the family of acrylic-based IP photoresists is 1000 nm along the optical axis of the focusing objective and 400 nm resolution in the objective focal plane, with a minimal feature size of 160 nm [19]. The feature size of OrmoComp structures is down to 150 nm [20]. Feature size of SZ2080 structures has been found to be 5% smaller than that of IP-Dip structures [21].

Post-processing technique – pyrolysis – simultaneously provides resolution enhancement with introducing new functionalities. Slow heating in an inert atmosphere eliminates organic parts and turns the material into either a glassy carbon or ceramics [22,23], depending on the precursor. The pyrolyzed materials have demonstrated high thermal and radiation stability [23–26] along with increased mechanical strength [27]. TPP with a subsequent pyrolysis has been successfully applied to make carbon nanoelectrodes for neurotransmitter sensing [28], custom tips [29] for atomic force microscopy, photonic crystals in visible range [30,31], and ultrastrong mechanical metamaterials [32,33]. A series of previous studies in this field have addressed the resolution enhancement by pyrolysis [21,30,32,34–36] and calcination [37,38] with the ratio of shrinkage down to 10% of initial size. However, a closer look at the literature reveals that it is hard to compare the results of experiments conducted in different conditions and evaluate important parameters for resolution enhancement. As previously reported in the literature [39], the structure's shrinkage is determined by a polymer precursor as well as the pyrolysis temperature, atmosphere, and geometry of the printed structure.

The byproduct of TPP exposure is residual stress that causes non-uniform shrinkage and delamination of the structures from the substrate [40]. The subsequent pyrolysis makes the adhesion problem even more challenging [41]. Despite the apparent practical significance of this question, only a few studies have addressed it systematically. The researchers have measured the adhesion forces between TPP-made microstructures and glass surfaces with and without an adhesion promoter just recently [42].

In this paper, we performed a comparative analysis of three commercially available photoresists – IP-Dip, OrmoComp, and SZ2080 – as precursors for TPP with subsequent pyrolysis. We used an X-ray lens on a pedestal [17,43] as a printed model object. Structures' elemental composition, shrinkage, and adhesion to the substrate were studied as a function of pyrolysis temperature.

2. Materials and methods

We have selected three commonly used photoresists for printing by TPP, which differ significantly in properties and chemical composition. IP-Dip is widely used for printing high-resolution structures by commercial Nanoscribe printer. IP-Dip is suitable as a material for X-ray optics [14,44], and IP-Dip structures have been successfully pyrolyzed before [21,30,32]. OrmoComp is a biocompatible material used for printing optical elements for the visible light, and is promising as a material for the X-ray optics as well [14,17,43]. There is no reference information about OrmoComp structures treated by pyrolysis. However, according to Fraunhofer Institute for Silicate research [45], some experiments were successfully performed on making nanoporous SiO₂ hollow fibers from ORMOCER photoresists by pyrolysis. SZ2080 is low shrinkage photoresist excellent for high resolution printing by TPP [46]. This photoresist turns into ceramics during pyrolysis [36,37], which might be useful for the purposes that require high stability under extreme irradiation. Seniutinas *et al.* [21] showed that dimensions of structural elements as well as the size of the entire printed structure could be controlled at the nanoscale by combining isotropic plasma etching and pyrolysis as post processing steps for IP-Dip and SZ2080.

All structures made of these photoresists were printed on the 500- μm -thick silicon wafer. The substrates were cleaned with acetone, isopropyl alcohol, and distilled water and afterwards placed in the piranha solution [47] for 30 minutes with the following distilled water rinsing and drying.

2.1. Materials

IP-Dip is a TPP-specialized organic negative-tone photoresist produced by Nanoscribe GmbH. *IP-Dip*'s molecular formula is $\text{CH}_2\text{N}_{0.001}\text{O}_{0.34}$ [48]. This resin contains 60–80% of pentaerythritol triacrylate (PETA). This photoresist is a fluid medium designed for dip-in laser lithography [49]. According to the provider's datasheet, the refractive index of unexposed material at the wavelength of 780 nm is 1.52, perfectly matching the focusing optics. The refractive index of polymerized photoresist is approximately 1.53 at 780 nm, depending on UV-exposure time and intensity [50]. *IP-Dip* was drop-casted on a silicon wafer and used according to the standard operating procedures provided by Nanoscribe [51]. The structures made of *IP-Dip* were developed by placing in PGMEA (supplied by Sigma-Aldrich) for 25 minutes with the following treatment in isopropyl alcohol (with 99% chemical purity) for 5 minutes. *IP-Dip* has numerous advantages: superior resolution, dip-in operation mode (allowing printing high structures easily), organic components that carbonize under pyrolysis.

OrmoComp is a hybrid organic-inorganic photoresist produced by Microresist Technology GmbH. Its molecular formula is $\text{C}_{21}\text{SO}_8\text{SiH}_{36}$ [43]. *OrmoComp* belongs to organically modified ceramics (ORMOCER) commonly prepared by sol-gel processing. The polymer's refractive index is approximately 1.513 at 780 nm [50,52]. *OrmoComp* is a high viscous liquid. Though it is possible to use *OrmoComp* in a dip-in operation mode for TPP, we applied standard operation mode, with oil immersion between the objective and the sample. The sample represented a cell with an *OrmoComp* layer placed between silicon and glass substrates. *OrmoComp* droplet was deposited on the silicon substrate and covered with a glass coverslip to make a cell. A stack of duct tape pieces (produced by Brauberg company) controlled the cell's height. One duct tape layer had a thickness of approximately 40 μm . We used three duct tape layers to make cells with a height of 120 μm . More details of the sample preparation can be found elsewhere [14]. After TPP exposure, the cells were immersed in methyl isobutyl ketone for 2 hours to remove the untreated photoresist and rinsed with isopropyl alcohol.

SZ2080 is a hybrid organic-inorganic sol-gel photoresist produced by IESL—FORTH, Greece [53]. Its polymer network resembles *OrmoComp* with some Si and N atoms replaced with Zr atoms, with chemical formula $\text{C}_4\text{H}_{12}\text{SiZrO}_2$ [54]. The zirconium additive hardens the polymerized resin. The refractive index of *SZ2080* is 1.5 at the wavelength of 632.8 nm [46]. However, Žukauskas *et al.* [55] found that TPP processing parameters, such as laser intensity and scanning velocity, can variate the refractive index of up to 1%, i.e., $\Delta n = 0.015$. A droplet of *SZ2080* resin was deposited on the silicon wafer and pre-baked at 100°C for 100 minutes. After the prebake step, the second layer of the resist was placed on the first one and covered with a glass in order to create a cell and dried on a hotplate at 100°C for 100 minutes to condensate the hydroxy mineral moieties and form an inorganic matrix. This pre-processing hardens photoresist material, that facilitates precise TPP manufacturing on the *SZ2080* workpiece. *SZ2080* structures were developed in methyl isobutyl ketone for 2 hours, likewise *OrmoComp* cells.

2.2. Fabrication of structures by two-photon polymerization

TPP was performed on two different setups. *IP-Dip* and *OrmoComp* structures were exposed by using Nanoscribe Photonic Professional. *SZ2080* and other *OrmoComp* structures were printed on a home-built TPP setup. We used Ti-Sapphire Chameleon Coherent femtosecond laser with the 80 MHz pulse rate and 780 nm wavelength. Plan-apochromat LD LCI 25×/NA0.8 or 100×/NA1.3 objective lenses focused laser radiation. Two-axis fast steering mirror (FSM-300-M-01, Newport corporation) deflected light to move the focal spot in the lateral plane. More details can be found in Ref. [43]. The laser power varied from 5 to 14 mW, depending on the photoresist material and laser velocity. The latter was approximately 300 $\mu\text{m/s}$ for Nanoscribe (PS3 option) and 900 $\mu\text{m/s}$ for the home-built setup. Both hatching and slicing distances were 0,2 μm .

The same X-ray lens on the high pedestal was used as a printing model for all three photoresists (see Fig. 1). This is a model of bi-concave parabolic refractive lens, which can be used for X-ray focusing. The lens model has been chosen due to its non-trivial shape, which allowed us to evaluate pyrolysis influence on geometric parameters and elemental composition. Table 2 specifies the model's main parameters. The lens has a parabolic radius of $5 \mu\text{m}$, a round aperture of $28 \mu\text{m}$, length, width, and height of $40,2 \times 34 \times 30 \mu\text{m}^3$, correspondingly. The lens is placed on a pedestal with a height of $50 \mu\text{m}$. This kind of structure's support is necessary to eliminate the influence of substrate during pyrolysis; the substrate does not shrink during pyrolysis, therefore the adhesion forces would also prevent the structure's bottom layers from shrinking. The higher layers would shrink less than expected until the certain height, from which the uniform shrinkage is observed. Fabrication of a single whole lens with a pedestal using the home-built setup in galvo scan mode takes approximately one hour. When using Nanoscribe, the lenses were printed in a piezo scan mode. Therefore, in order to shorten the printing time, the lens and the pedestal were printed separately. In the piezo scan mode with the aforementioned printing settings, the fabrication of one lens without a pedestal takes approximately 4 hours. The pedestal has been printed in shell&scaffold fill mode, in which solely framework of the pedestal is printed with $5 \mu\text{m}$ -thick walls. The printing time of the pedestal in these conditions reaches approximately 20 minutes. In the solid fill mode (used to print the lens), the fabrication time of one pedestal by Nanoscribe is estimated to be of 8 hours. During the development process, these structures with hollow pedestals were treated with UV radiation to polymerize the photoresist material inside the pedestal. For UV-curing, the structures were irradiated for 30 minutes using high-pressure mercury-vapor lamp. The radiation intensity was 12 mW/cm^2 in the spectral range of 280-400 nm.

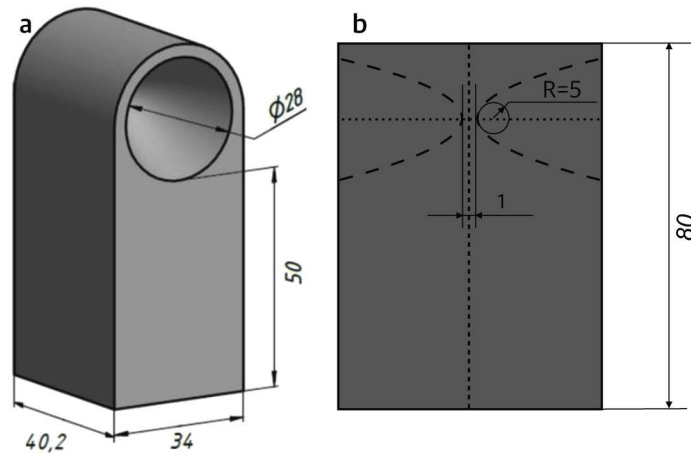


Fig. 1. Model of X-ray lens on solid pedestal, all sizes are in μm : a - 3D view, b - vertical cross-section along the optical axis of the lens

In most of the previous works, the pyrolyzed structures had rod lattice. Though this lattice design is highly efficient, various, especially optical, applications require solid-state microstructures. Additionally, solid-state structures are better suited for measuring elemental composition and adhesion.

2.3. Pyrolysis

The pyrolysis was performed in a horizontal tube furnace (SNOL, NPO Tehnokom) under the constant argon flow (approximately 30 ml per minute). The process includes three stages:

- heating from room temperature to peak temperature with a constant heat rate of 1.5°C per minute;
- keeping the sample under peak temperature for a dwell time of 30 minutes;
- switching off the furnace and cooling down to room temperature, which takes several hours;

According to literature, peak temperature in post-processing varies significantly, from 300°C [56] up to 1500°C [37]. We relied on thermogravimetric analysis (TGA) to choose two pyrolysis temperatures out of this range. Figure 2 shows the temperature-dependent mass loss of the SZ2080 material. SZ2080 polymer film was produced by the standard protocol, but it was exposed to the UV radiation and separated from the substrate instead of TPP processing. For UV-curing, the films were irradiated for 24 hours with the radiation intensity of 25 mW/cm² in the spectral range of 280-400 nm. The measurements were performed on NETZSCH STA 449 device (NETZSCH-Gerätebau GmbH), combined with QMS 409 mass-spectrometer. The SZ2080 material was heated in argon flow (30 ml per minute) with a heat ramp of 5°C per minute in the range from 40 to 1000°C. The mass loss and its derivative are shown on the left panel. The mass loss slightly decreases from the initial temperature, which indicates the removal of the partially cross-linked resin (or unreacted resin) within the cured SZ2080. The polymer starts to decompose at 360°C. The mass loss derivative allowed us to determine the temperature of phase transitions. The most significant loss occurs at the temperature of 396°C, and additional extremum can be seen at 451°C. Total mass loss during thermal decomposition amounted to 44,2%. The right panel shows mass-spectrometric detection of common polymer decomposition products – H₂O, CO, CH₂O, CO₂. Stages of polymer decomposition detected from TGA correspond to the release of these products. At the first stage, near 400°C, water, carbon monoxide, and carbon dioxide release. At the second stage near 450°C we observe a peak of CO release, among with reduced evaporation of H₂O and CO₂. Mass-spectrometry helps us to detect the third stage near 490°C with a small peak of formaldehyde evaporation and a continuous process of CO release. Thermal decomposition process stops at temperatures exceeding 600°C. To summarize, the most considerable mass reduction occurs in the range of 400-450°C.

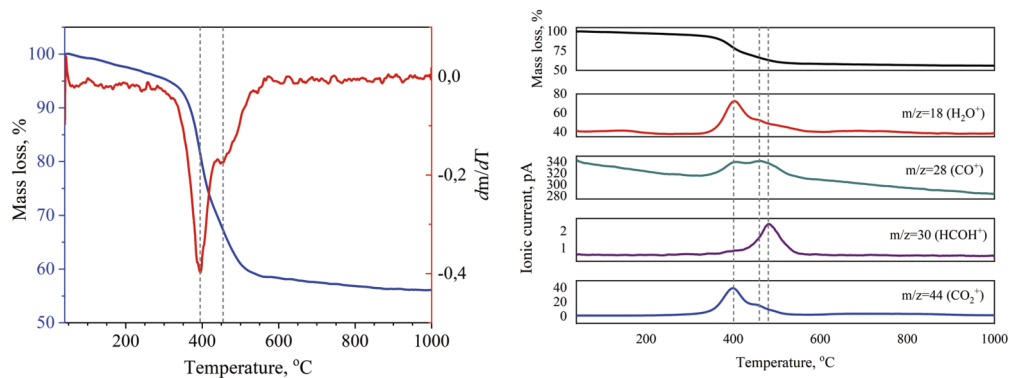


Fig. 2. Thermogravimetric analysis of SZ2080 photoresist. Left panel: mass loss (blue line) and mass loss derivative (red) during heating in Ar atmosphere. Right panel, top-to-down: TGA mass loss (black) and mass-spectrometric detection of decomposed components - H₂O (red), CO (green), CH₂O (violet), CO₂ (blue)

Similar results on IP-Dip and Ormocomp can be found in the other works. Ormocomp's thermal decomposition starts at 360°C with the major mass loss within the range of 400-500°C [57]. Mass reduction stops at 500°C with 15% of the initial mass remained. TGA of IP-Dip [30]

shows a similar curve with extremum of mass loss at 450°C. Because of the major mass loss at 450°C for all three photoresists, we expected both a uniform shrinkage of the printed structure and a significant loss of the organic part of the material, which is particularly appealing for many applications, especially manufacturing the X-ray optics. Based on this data, we have chosen first pyrolysis temperature point of 450°C.

According to TGA, at temperatures exceeding 600°C, mass loss almost completely stops for all photoresists under study, indicating that all the organic components have been released, and the material's elemental compound becomes stable. Therefore, any pyrolysis temperature in the 600°C-1000°C range is expected to lead to the same elemental compound and the resemblant value of shrinkage ratio. It was reasonable to choose the second pyrolysis temperature point near the lowest threshold and we picked 690°C, as there is already some research on pyrolysis of IP-Dip and SZ2080 TPP-made structures for this temperature [21].

To summarize, based on the TGA data and the pertinent literature, we have selected two peak temperatures for the pyrolysis process: 450°C, 690°C.

2.4. Characterization of printed structures

The printed structures were characterized before and after pyrolysis by scanning electron microscopy (SEM) performed on Nova NanoSEM 230 microscope. We have also performed X-ray energy dispersive analysis (EDX) to find out the changes in the elemental composition of the photoresists. EDX analyzer (Bruker company) has been coupled with SEM microscope. EDX does not reveal light elements, such as hydrogen, helium, as well as probably lithium and beryllium [58]. Still, the method is useful and can be combined with SEM easily. The declared error of measurement is 15% of the value. As hydrogen is the lightest element and quickly evaporates with the temperature increase, we assumed that there is no hydrogen in the pyrolyzed structures.

3. Results and discussions

Tables 1–3 summarize the obtained results. Table 1 presents photoresists' elemental analysis before and after pyrolysis made by energy-dispersive X-ray spectroscopy (EDX). The expected values in Table 1 are calculated from the polymer's molecular formulae. The rest data were obtained by EDX of the printed structures before and after pyrolysis. The values before pyrolysis are in good agreement with the expected values in despite EDX low accuracy. After pyrolysis, the elemental composition changes, which shows the partial release of some elements.

Table 2 shows shrinkage parameters calculated from the SEM images. As expected, the structures shrunk after pyrolysis. Using the SEM images, we measured the structures' geometric parameters, i.e., width, length, height, and aperture diameters, for all pyrolyzed and non-pyrolyzed structures that remained on the substrate, and these values were averaged to characterize the shrinkage parameters as one of the pyrolysis results.

3.1. IP-Dip

According to EDX (see Table 1), the initial structure contained 77.5% carbon and 22.5% oxygen. Meanwhile, the structures pyrolyzed at 450°C consist of carbon by 94%, while just 6% of oxygen persists. Therefore pyrolysis at 450°C turns IP-Dip structures into amorphous carbon with a slight additive of oxygen impurities. Further temperature increase might help remove the residual oxygen and turn IP-Dip into pure glassy carbon.

Figure 3 shows SEM images of IP-Dip lens before (a) and after (b) pyrolysis at 450°C. All scale bars are 20 μm. Out of 16 printed structures 15 lenses survived pyrolysis. The pyrolyzed lens demonstrated the shrinkage of the linear size for up to 2.1 times. Previously [30,32], 5x size reduction of IP-Dip structures has been demonstrated. However, shrinkage is size-dependent and is more prominent for narrow and thin structures. We pyrolyzed solid structures in our work,

Table 1. Elemental analysis of IP-Dip, OrmoComp, and SZ2080 structures before and after pyrolysis with peak temperatures of 450°C and 690°C.

Photoresist	C, at. %	O, at. %	N, at. %	Si, at. %	Zr, at. %	S, at. %
IP-Dip						
Expected	74.57	25.35	0.08	0	0	0
Before	77.5	22.5	0	0	0	0
After 450°C	94	6	0	0	0	0
Ormocomp						
Expected	68	26	0	3	0	3
Before	67	26	0	4	0	3
After 450°C	44	43	0	13	0	0
After 690°C	3	70	0	27	0	0
SZ2080						
Expected	43	45	0	10	2	0
Before	43	45	0	10	2	0
After 450°	20	51	0	26	3	0
After 690°	3	66	0	30	1	0

Table 2. Shrinkage parameters.

		Length, μm	Width, μm	Height, μm	Aperture diameter, μm	Shrinkage ratio
Model dimensions		40.2	34	80	28	-
IP-Dip						
450°C	Before	40.1	34.9	80.6	24.3	-
	After	19.4	16.5	40.3	11.7	2.1
Ormocomp						
450°C	Before	40.1	33.8	78.1	21.7	-
	After	19.6	16.6	37.8	11.2	2.0
690°C	Before	40.2	34	79.1	28	-
	After	16.9	14.2	36.0	11.5	2.4
SZ2080						
690°C	Before	40.2	34	75.7	28	-
	After	25.3	21.5	43.4	16.6	1.6

Table 3. Comparison of pyrolyzed structures' key parameters: shrinkage and survival rate for pyrolysis temperatures of 450°C and 690°C, adhesion, pyrolyzed material.

Photoresist	Shrinkage ratio		Survival rate, %		Adhesion	Pyrolyzed Material
	450°C	690°C	450°C	690°C		
IP-Dip	2.1	-	94	0	moderate	glassy carbon
OrmoComp	2.0	2.4	100	100	good	glass
SZ2080	-	1.6	88	75	poor	Zr-doped glass

while the 5× shrinkage was achieved for the woodpile structures made of thin single-voxel rods with a diameter of approximately 0.5 μm . Additionally, shrinkage depends on the degree of cross-linking: structures with a high degree of cross-linking are less shrinkable [37]. We exposed our structures to UV-radiation during development to add mechanical stability to the pedestals. This treatment increased the cross-linking degree of the structures and therefore resulted in lesser shrinkage.

The shrinkage changes in the direction perpendicular to the substrate: shrinkage grows with the increase of distance from the substrate. This phenomenon is brought about by the structure-to-substrate mechanical stress and adhesion. The structure adhesion to the silicon substrate is strong enough to hold the pedestal's lower layers and prevent the same shrinkage as in the upper part of the lens. The influence of the substrate is observed for the pyrolyzed structure up to the height of 10 μm . At higher altitudes, the structures shrink isotropically. The microstructure's adhesion deteriorates along with pyrolysis: while the base of the unpyrolyzed structure is fully connected to the substrate, after pyrolysis, the edges of the pedestal base are visibly lifted above the substrate. This implies that the pedestal base is partially detached from the substrate due to pyrolysis.

We also performed the pyrolysis of the IP-Dip lenses at 690°C, but no structures remained at the substrate. The latter can be explained by the strong impact of pyrolysis on adhesion: the adhesion worsens at higher temperatures; therefore, the structures detach from the substrate.

3.2. OrmoComp

The elemental compound of OrmoComp structures before and after pyrolysis is presented in Table 1. The initial material contained 67% carbon, 30% silicon, and 66% oxygen. Pyrolysis at 450°C leads to 44% carbon, 13% silicon, and 43% oxygen. The lens pyrolyzed at 690°C consists of 3% carbon, 30% silicon, and 66% oxygen. As we see, the amount of carbon drops with the temperature, while percentages of silicon and oxygen rise. The temperature of 450°C is not high enough to remove the carbon-containing substances from the OrmoComp structure. After pyrolysis at 690°C we can state that the obtained material consists of SiO_2 with a small fraction of carbon inclusions. This fact is in good agreement with TGA, which indicated final mass loss at 500°C and led to the dramatic shrinkage ratio increase with the temperature rising.

Figure 3 (c,d,e) shows SEM images of OrmoComp lens before pyrolysis (a) and after pyrolysis at 450°C (b) and 690°C (c). All printed lenses successfully survived pyrolysis at both temperatures. The shrinkage ratio grows from 2.0 at 450°C to 2.4 at 690°C (see Table 1). Similar to IP-Dip structures in Fig. 3(a,b), one can notice height-dependent shrinkage near the substrate caused by the structure's adhesion to the substrate. The structures shrink isotropically at the altitudes higher than 18 μm . The latter height value relates to pyrolyzed structures, which can be translated to the height of 36-44 μm for the initial structures. In contrast with IP-Dip structures, the adhesion of OrmoComp structures does not change, regardless of the pyrolysis temperature. The structures before and after pyrolysis at 450°C and 690°C are equally well connected to the substrate.

We carried out a separate experiment with the pedestal to find out the height of isotropic shrinkage. In this experiment, we pyrolyzed at the temperature of 690°C the parallelepipeds with 34×40.2 μm base, coinciding with the sizes of lens' base, and a height of 30, 40, and 50 μm . Figure 4 shows SEM images of pyrolyzed pedestals. The structures' size reduction is non-uniform along the vertical direction. The pedestal bases remained the same size after pyrolysis, which infers an excellent adhesion of OrmoComp structures to the silicon substrate. This strong adhesion holds the bottom pedestal layers and therefore prevents the structure from isotropic shrinkage. The deformations of the pedestal caps illustrate shrinkage at the designated height. The top edge of the 30- μm pedestal (left panel in Fig. 4) is bent dramatically. The 40- μm pedestal cap (center panel) is less curved, but a lack of flatness can still be observed. The 50 μm -thick pedestal (right panel) has a flat top edge. We observe the isotropic shrinkage of

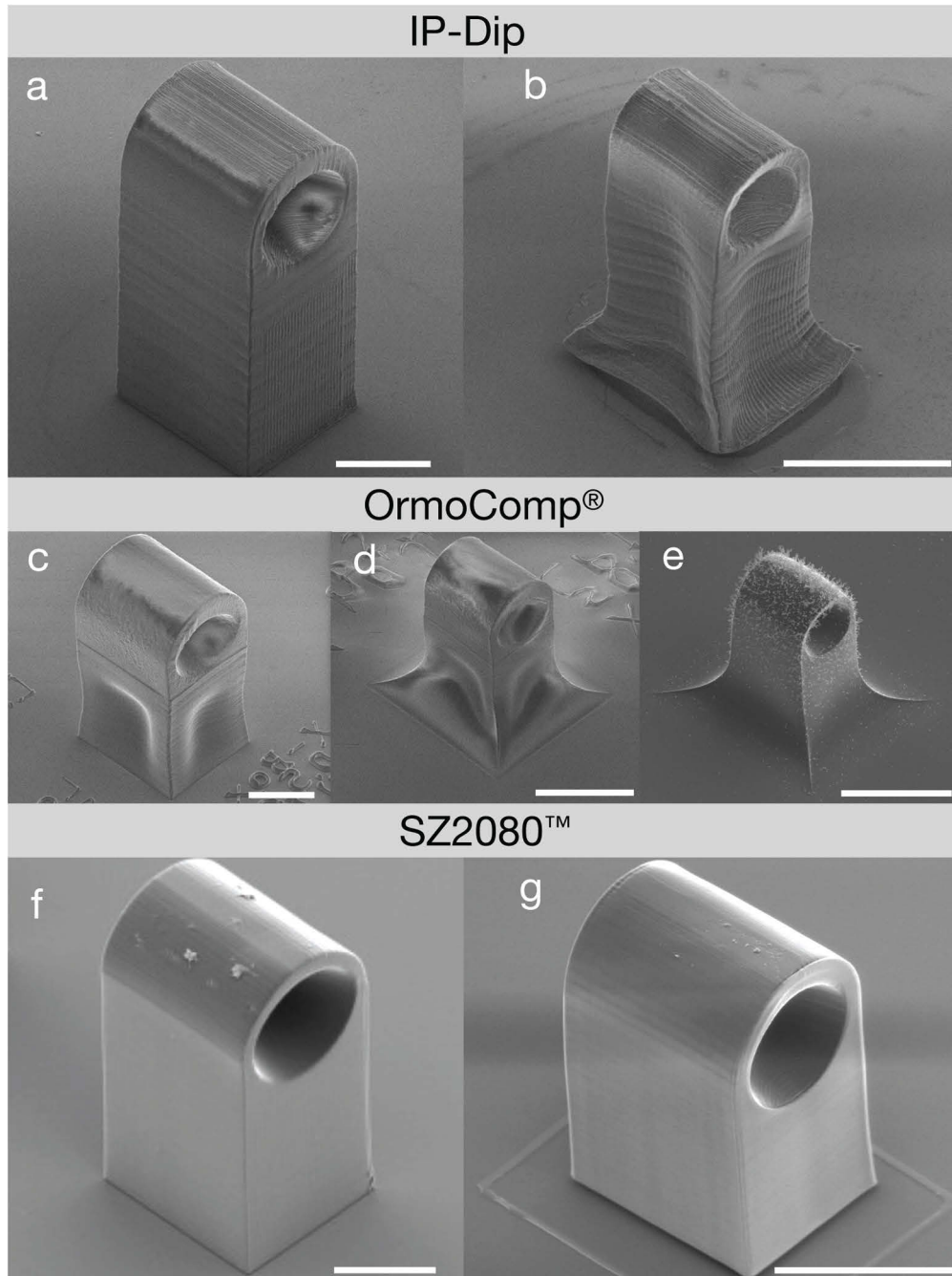


Fig. 3. SEM pictures of structures printed from IP-Dip, OrmoComp, and SZ2080. Upper row: IP-Dip lens (a) before pyrolysis, and (b) after pyrolysis at 450°C. Middle row: OrmoComp lens (c) before pyrolysis, and after pyrolysis at (d) 450°C and (e) 690°C. Bottom row: SZ2080 lens (f) before pyrolysis, and (f) after pyrolysis at 690°C. All scale bars are 20 μm .

50 μm -thick pedestal starting at a certain distance from the substrate. The height of isotropic shrinkage for initial structure equals 38 ± 3 μm . Based on these findings, conducted before the main experiments, we placed the structure's model on top of a solid pedestal with a height of 50 μm .

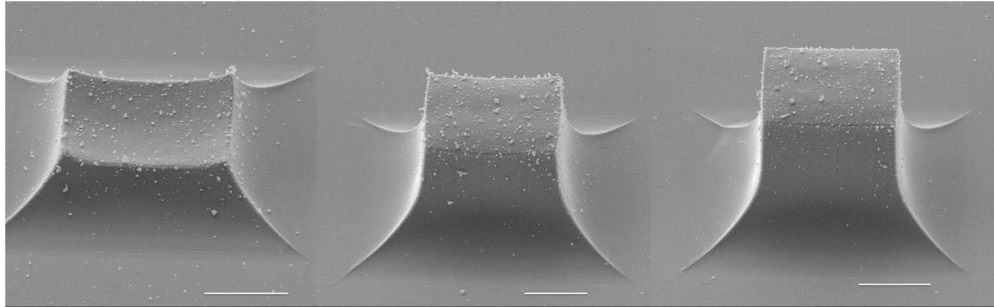


Fig. 4. SEM images of OrmoComp pedestals after pyrolysis at 690°C with 30 μm (left), 40 μm (center), and 50 μm (right) initial height; all three scale bars are 10 μm .

3.3. SZ2080

According to the TGA (see Fig. 2), we expect the resin's total conversion to the non-organic compound at 490-500°C. The elemental compound of the pyrolyzed SZ2080 structures is shown in Table 2. Initially, SZ2080 structures contained 43% carbon, 45% oxygen, 10% silicon, and 2% zirconium. The structures pyrolyzed at 450°C consisted of 20% of carbon, 51% of oxygen, 26% of silicon, and 3% of zirconium. After pyrolysis at 690°C the amount of carbon amounted to 3%, with 51% of oxygen, 26% of silicon, and 1% of zirconium. As the pyrolysis temperature increases, the percentage of carbon drops, while the amount of oxygen and silicon grows. SZ2080 photoresist turns mainly into SiO_2 during the pyrolysis at 690°C with small persistent amounts of carbon and zirconium. The transformation is not completed during the 450°C pyrolysis: the amount of carbon reaches 20%. This confirms that the temperature of 450°C is not high enough to remove the organic parts from the compound, as we see on TGA.

Figure 3 (f,g) demonstrates SEM images of a typical structure – lens on a high solid pedestal–made of SZ2080 before and after pyrolysis at 690°C. This lens successfully survived pyrolysis; however, only 75% of SZ2080 structures endured pyrolysis, and 35% of pyrolyzed structures have visible defects, such as cracks and hollows. In contrast, pyrolysis at 450°C does not induce the structures' damage. The shrinkage ratio at 690°C is 1.6 (see Table 2). The structures pyrolyzed at 450°C were not suitable to determine the shrinkage ratio, but viable to perform the elemental analysis.

In contrast with Ip-Dip and OrmoComp lenses, the SZ2080 lens demonstrates isotropic shrinkage of the whole structure, independent of the height. We also observe the gap between the lens and the substrate and a trace of the initial pedestal edges on the substrate after pyrolysis. These facts indicate poor adhesion, which leads to the 25% structures' loss. The result leads to a conclusion that SZ2080 is most suitable for the stand-alone structures and not recommended for the ordered arrays of structures printed on one substrate.

3.4. Discussion

Table 3 compares pyrolyzed structures made of IP-Dip, OrmoComp, and SZ2080, by three major parameters: shrinkage, elemental compound, and adhesion. OrmoComp demonstrated the best adhesion, independent of pyrolysis. The predictable shrinkage of OrmoComp structures, together with good adhesion and 100% survival rate, makes this photoresist promising for more

complex printing, for example, an ordered array of structures. This feature may be demanded for creating compound X-ray lenses [17], metasurfaces and other devices. On the other hand, the adhesion of SZ2080 is relatively weak. Poor adhesion of SZ2080 to silicon substrate determined that only a few SZ2080 structures successfully survived pyrolysis without falling or misplacing. Nevertheless, there is an advantage in poor adhesion: low structure-substrate interaction leads to the isotropic shrinkage. SZ2080 lenses shrunk uniformly, while OrmoComp and IP-Dip lenses' pedestals distorted in a non-linear manner in the area near the substrate. Therefore, the pyrolyzed structures made of SZ2080 can be useful if their orientation is insignificant, or, even better, free-standing structures are required. IP-Dip showed medium case: its adhesion is weaker than OrmoComp, but better than SZ2080. In our experiments, IP-Dip structures did not survive the pyrolysis at a temperature of 690°C. However, in previous studies IP-Dip structures have endured heating of up to 900°C [32]. Thus, high temperatures may be tangible with special preparation of the substrate's surface for better adhesion to photoresist structure, i.e., using an adhesion promoter.

Different resins demonstrate different shrinkage. Ip-Dip and OrmoComp show high shrinkage, while SZ2080 is harder to shrink. This tendency is consistent with the previous data on SZ2080 and Ip-Dip [21]. We explain this by inorganic hard silicon carcass, which remains persistent for OrmoComp and SZ2080. Inorganic components lower the shrinkage of the pyrolyzed resins, especially for Zr-enforced SZ2080 carcass. The temperature of 450°C allows one to achieve isotropic shrinking in the range of 2.0-2.1 for different photoresists. As the pyrolysis temperature increases up to 690°C, the shrinkage grows up to 25%: 2.4 for OrmoComp and 1.6 for SZ2080.

The EDX results show that the Ip-Dip turns mainly into glassy carbon during pyrolysis. This transformation is almost complete at 450°C, which is seen by the increased amount of carbon atoms with a decreased amount of oxygen atoms in elemental analysis. The glassy carbon possesses good electrical conductivity and has a wide range of applications, such as 3D free-form electrodes [28,59] and durable mechanical metamaterials [10,32,60]. OrmoComp and SZ2080 transform into silicon dioxide with nearly stoichiometric compound at 690°C. This transformation occurs because of carbon removal. The amount of released carbon increases with the pyrolysis temperature.

4. Conclusions

We have pyrolyzed polymer structures made by TPP and analyzed the effect of pyrolysis on elemental composition, shrinking and adhesion. IP-Dip turns into glassy carbon after pyrolysis at 450°C, while OrmoComp and SZ2080 turn mainly into SiO₂ at 690°C. Out of the three examined photoresists, OrmoComp demonstrates the best adhesion, SZ2080 the worst, and IP-Dip the medium one. The adhesion quality correlates directly with the structures' survival rate under pyrolysis and the observed height of isotropic shrinkage. Organic IP-Dip is more shrinkable than organic-inorganic SZ2080 and OrmoComp, and size reduction grows with the pyrolysis temperature. Structures made of SZ2080 shrink uniformly, while OrmoComp and IP-Dip structures have uniform shrinkage starting at some level from the substrate. As the pyrolysis temperature increases up to 690°C, the shrinkage grows up to 25%: 2.4 for OrmoComp and 1.6 for SZ2080. Though there is no evidence that TPP-printed OrmoComp structures were pyrolyzed before, in this research OrmoComp demonstrated a good fit for pyrolysis.

The results of the current work have straightforward application in material science and can provide a starting point for any research that involves additive manufacturing with pyrolysis post-processing.

Funding. Russian Science Foundation (20-12-00371); Russian Foundation for Basic Research and Moscow City Government grant (15-12-00065); Russian Foundation for Basic Research (18-02-00811, 18-29- 20129); Ministry of Science and Higher Education of the Russian Federation (14.W03.31.0008); MSU Quantum Technology Center.

Acknowledgments. The authors thank S. Sokolov (Institute of Nanotechnology of Microelectronics of the Russian Academy of Sciences) for making SEM images and M. Lyubomirskiy (Deutsches Elektronen-Synchrotron DESY) for fruitful discussions. The authors are grateful to Mr. R.D. Zvagelsky (MIPT, #3D-lab) for assistance with DLW procedure. M.I. Sharipova thanks Prof. Yang (Singapore University of Technology and Design) for the detailed response regarding the manufacturing of structural color 3D photonic crystals.

Disclosures. The authors declare no conflicts of interest.

References

1. M. Farsari and B. N. Chichkov, "Two-photon fabrication," *Nat. Photonics* **3**(8), 450–452 (2009).
2. X. Zhou, Y. Hou, and J. Lin, "A review on the processing accuracy of two-photon polymerization," *AIP Adv.* **5**(3), 030701 (2015).
3. H. Zeng, P. Wasylczyk, C. Parmeggiani, D. Martella, M. Burrelli, and D. S. Wiersma, "Light-fueled microscopic walkers," *Adv. Mater.* **27**(26), 3883–3887 (2015).
4. T. Ergin, N. Stenger, P. Brenner, J. B. Pendry, and M. Wegener, "Three-dimensional invisibility cloak at optical wavelengths," *Science* **328**(5976), 337–339 (2010).
5. T. Gissibl, S. Thiele, A. Herkommer, and H. Giessen, "Two-photon direct laser writing of ultracompact multi-lens objectives," *Nat. Photonics* **10**(8), 554–560 (2016).
6. P.-I. Dietrich, M. Blaicher, I. Reuter, M. Billah, T. Hoose, A. Hofmann, C. Caer, R. Dangel, B. Offrein, U. Troppenz, M. Moehle, W. Freude, and C. Koos, "In situ 3D nanoprinting of free-form coupling elements for hybrid photonic integration," *Nat. Photonics* **12**(4), 241–247 (2018).
7. K. R. Safronov, D. N. Gulkin, I. M. Antropov, K. A. Abrashitova, V. O. Bessonov, and A. A. Fedyanin, "Multimode interference of Bloch surface electromagnetic waves," *ACS Nano* **14**(8), 10428–10437 (2020).
8. M. Malinauskas, A. Žukauskas, V. Purlys, A. Gaidukevičius, Z. Balevičius, A. Piskarskas, C. Fotakis, S. Pissadakis, D. Gray, R. Gadonas, M. Vamvakaki, and M. Farsari, "3D microoptical elements formed in a photostructurable germanium silicate by direct laser writing," *Optics and Lasers in Engineering* **50**(12), 1785–1788 (2012).
9. J. Serbin, A. Egbert, A. Ostendorf, B. Chichkov, R. Houbertz, G. Domann, J. Schulz, C. Cronauer, L. Fröhlich, and M. Popall, "Femtosecond laser-induced two-photon polymerization of inorganic–organic hybrid materials for applications in photonics," *Opt. Lett.* **28**(5), 301–303 (2003).
10. T. Bückmann, N. Stenger, M. Kadic, J. Kaschke, A. Frölich, T. Kennerknecht, C. Eberl, M. Thiel, and M. Wegener, "Tailored 3D mechanical metamaterials made by dip-in direct-laser-writing optical lithography," *Adv. Mater.* **24**(20), 2710–2714 (2012).
11. H. Wei, M. Chen, and S. Krishnaswamy, "Three-dimensional-printed Fabry–Perot interferometer on an optical fiber tip for a gas pressure sensor," *Appl. Opt.* **59**(7), 2173–2178 (2020).
12. E. D. Lemma, B. Spagnolo, M. De Vittorio, and F. Pisanello, "Studying cell mechanobiology in 3D: the two-photon lithography approach," *Trends Biotechnol.* **37**(4), 358–372 (2019).
13. Z.-C. Ma, Y.-L. Zhang, B. Han, X.-Y. Hu, C.-H. Li, Q.-D. Chen, and H.-B. Sun, "Femtosecond laser programmed artificial musculoskeletal systems," *Nat. Commun.* **11**(1), 4536 (2020).
14. M. Lyubomirskiy, F. Koch, K. A. Abrashitova, V. O. Bessonov, N. Kokareva, A. Petrov, F. Seiboth, F. Wittwer, M. Kahnt, M. Seyrich, A. A. Fedyanin, C. David, and C. G. Schoer, "Ptychographic characterisation of polymer compound refractive lenses manufactured by additive technology," *Opt. Express* **27**(6), 8639–8650 (2019).
15. F. Seiboth, D. Brückner, M. Kahnt, M. Lyubomirskiy, F. Wittwer, D. Dzhigaev, T. Ullsperger, S. Nolte, F. Koch, C. David, J. Garrovoet, G. Falkenberg, and C. G. Schroer, "Hard X-ray wavefront correction via refractive phase plates made by additive and subtractive fabrication techniques," *J. Synchrotron Radiat.* **27**(5), 1121–1130 (2020).
16. A. Mikhaylov, S. Reich, M. Zakharova, V. Vlnieska, R. Laptev, A. Plech, and D. Kunka, "Shack–Hartmann wavefront sensors based on 2D refractive lens arrays and super-resolution multi-contrast x-ray imaging," *J. Synchrotron Radiat.* **27**(3), 788–795 (2020).
17. A. Barannikov, M. Polikarpov, P. Ershov, V. Bessonov, K. Abrashitova, I. Snigireva, V. Yunkin, G. Bourenkov, T. Schneider, A. A. Fedyanin, and A. Snigirev, "Optical performance and radiation stability of polymer X-ray refractive nano-lenses," *J. Synchrotron Radiat.* **26**(3), 714–719 (2019).
18. A. Pikulin and N. Bityurin, "Fluctuation limitations on the voxel minimal size at laser nanopolymerization," *Tech. Phys.* **57**(5), 697–705 (2012).
19. GmbH Nanoscribe, "Nanoscribe Photonic Professional GT2," <https://www.nanoscribe.com/en/products/photonic-professional-gt2#tab-385>.
20. J. Serbin and M. Gu, "Superprism phenomena in waveguide-coupled woodpile structures fabricated by two-photon polymerization," *Opt. Express* **14**(8), 3563–3568 (2006).
21. G. Seniutinas, A. Weber, C. Padeste, I. Sakellari, M. Farsari, and C. David, "Beyond 100 nm resolution in 3D laser lithography — Post processing solutions," *Microelectron. Eng.* **191**, 25–31 (2018).
22. A. Vyatskikh, "Additive manufacturing of 3D nano-architected metals and ceramics," Ph.D. thesis, California Institute of Technology (2020).
23. O. J. Schueller, S. T. Brittain, and G. M. Whitesides, "Fabrication of glassy carbon microstructures by pyrolysis of microfabricated polymeric precursors," *Adv. Mater.* **9**(6), 477–480 (1997).
24. Y. Tang, J. Wang, X. Li, W. Li, H. Wang, and X. Wang, "Thermal stability of polymer derived SiBNC ceramics," *Ceram. Int.* **35**(7), 2871–2876 (2009).

25. F. Zhang, J. Ilavsky, G. G. Long, J. P. Quintana, A. J. Allen, and P. R. Jemian, "Glassy carbon as an absolute intensity calibration standard for small-angle scattering," *Metall. Mater. Trans. A* **41**(5), 1151–1158 (2010).
26. J. Rossbach, J. R. Schneider, and W. Wurth, "10 years of pioneering X-ray science at the Free-Electron Laser FLASH at DESY," *Phys. Rep.* **808**, 1–74 (2019).
27. J. Bauer, A. G. Izard, Y. Zhang, T. Baldacchini, and L. Valdevit, "Thermal post-curing as an efficient strategy to eliminate process parameter sensitivity in the mechanical properties of two-photon polymerized materials," *Opt. Express* **28**(14), 20362–20371 (2020).
28. C. Yang, Q. Cao, P. Puthongkham, S. T. Lee, M. Ganesana, N. V. Lavrik, and B. J. Venton, "3D-Printed Carbon Electrodes for Neurotransmitter Detection," *Angew. Chem. Int. Ed.* **57**(43), 14255–14259 (2018).
29. A. Zakhurdaeva, P.-I. Dietrich, H. Hölscher, C. Koos, J. G. Korvink, and S. Sharma, "Custom-designed glassy carbon tips for atomic force microscopy," *Micromachines* **8**(9), 285 (2017).
30. Y. Liu, H. Wang, J. Ho, R. C. Ng, R. J. Ng, V. H. Hall-Chen, E. H. Koay, Z. Dong, H. Liu, C.-W. Qiu, J. R. Greer, and J. K. W. Yang, "Structural color three-dimensional printing by shrinking photonic crystals," *Nat. Commun.* **10**(1), 4340 (2019).
31. S. Passinger, M. S. Saifullah, C. Reinhardt, K. R. Subramanian, B. N. Chichkov, and M. E. Welland, "Direct 3D patterning of TiO₂ using femtosecond laser pulses," *Adv. Mater.* **19**(9), 1218–1221 (2007).
32. J. Bauer, A. Schroer, R. Schwaiger, and O. Kraft, "Approaching theoretical strength in glassy carbon nanolattices," *Nat. Mater.* **15**(4), 438–443 (2016).
33. C. Crook, J. Bauer, A. G. Izard, C. S. de Oliveira, J. M. d. S. e Silva, J. B. Berger, and L. Valdevit, "Plate-nanolattices at the theoretical limit of stiffness and strength," *Nat. Commun.* **11**(1), 1579 (2020).
34. B. Cardenas-Benitez, C. Eschenbaum, D. Mager, J. G. Korvink, M. J. Madou, U. Lemmer, I. De Leon, and S. O. Martinez-Chapa, "Pyrolysis-induced shrinking of three-dimensional structures fabricated by two-photon polymerization: experiment and theoretical model," *Microsyst. Nanoeng.* **5**(1), 38 (2019).
35. Y. Daicho, T. Murakami, T. Hagiwara, and S. Maruo, "Formation of three-dimensional carbon microstructures via two-photon microfabrication and microtransfer molding," *Opt. Mater. Express* **3**(6), 875–883 (2013).
36. L. Jonušauskas, D. Gailevičius, L. Mikoliūnaitė, D. Sakalauškas, S. Šakirzanovas, S. Juodkazis, and M. Malinauskas, "Optically clear and resilient free-form μ -optics 3D-printed via ultrafast laser lithography," *Materials* **10**(1), 12 (2017).
37. D. Gailevičius, V. Padolskytė, L. Mikoliūnaitė, S. Šakirzanovas, S. Juodkazis, and M. Malinauskas, "Additive-manufacturing of 3D glass-ceramics down to nanoscale resolution," *Nanoscale Horiz.* **4**(3), 647–651 (2019).
38. N. Chai, Y. Liu, Yu. Yue, P. Wei, X. Wang, J. Zhao, Q. Zhang, F. Huang, Zh. Zeng, Z. Gan, L. Mai, and Yi. Cheng, "Tin Oxide Ceramics 3D Nonlinear Photolithography via Femtosecond Laser," <https://doi.org/10.1007/s40843-020-1543-x>.
39. R. Natu, M. Islam, J. Gilmore, and R. Martinez-Duarte, "Shrinkage of SU-8 microstructures during carbonization," *J. Anal. Appl. Pyrolysis* **131**, 17–27 (2018).
40. A. A. Bauhofer, S. Krödel, J. Rys, O. R. Bilal, A. Constantinescu, and C. Daraio, "Harnessing photochemical shrinkage in direct laser writing for shape morphing of polymer sheets," *Adv. Mater.* **29**(42), 1703024 (2017).
41. A. Singh, J. Jayaram, M. Madou, and S. Akbar, "Pyrolysis of negative photoresists to fabricate carbon structures for microelectromechanical systems and electrochemical applications," *J. Electrochem. Soc.* **149**(3), E78 (2002).
42. A. Izard, E. Garcia, M. Dixon, E. Potma, T. Baldacchini, and L. Valdevit, "Enhanced adhesion in two-photon polymerization direct laser writing," *AIP Adv.* **10**(4), 045217 (2020).
43. A. K. Petrov, V. O. Bessonov, K. A. Abrashitova, N. G. Kokareva, K. R. Safronov, A. A. Barannikov, P. A. Ershov, N. B. Klimova, I. I. Lyatun, V. A. Yunkin, M. Polikarpov, I. Snigireva, A. A. Fedyanin, and A. Snigirev, "Polymer X-ray refractive nano-lenses fabricated by additive technology," *Opt. Express* **25**(13), 14173–14181 (2017).
44. M. Mirzaeimoghri, A. Morales Martinez, A. Panna, E. E. Bennett, B. M. Lucotte, D. L. DeVoe, and H. Wen, "Nano-printed miniature compound refractive lens for desktop hard x-ray microscopy," *PLoS One* **13**(8), e0203319 (2018).
45. Microresist technologies, "ORMOCER® (hollow) fibers and nanoporous SiO₂ hollow fibers," https://www.ormocere.de/en/applications/omocers-as-bulk-materials/ormocer_hollow_fibers.html.
46. A. Ovsianikov, J. Viertel, B. Chichkov, M. Oubaha, B. MacCraith, I. Sakellari, A. Giakoumaki, D. Gray, M. Vamvakaki, M. Farsari, and C. Fotakis, "Ultra-low shrinkage hybrid photosensitive material for two-photon polymerization microfabrication," *ACS Nano* **2**(11), 2257–2262 (2008).
47. P. Stevic, "Piranha Cleaning Standard Operating Procedure," <https://d1rkab7tlqy5f1.cloudfront.net/TNW/Afdelingen/Quantum>
48. O. Stein, Y. Liu, J. Streit, R. Cahayag, Y. Lu, and N. Petta, "Handling and assembling of low-density foam structures fabricated by two-photon polymerization," *Nanoengineering: Fabrication, Properties, Optics, and Devices XIV*, vol. 10354 (International Society for Optics and Photonics, 2017), p. 103540L.
49. A. Pisarenko, R. Zvagelsky, D. Kolymagin, B. Katanchiev, A. Vitukhnovsky, and D. Chubich, "DLW-printed optical fiber micro-connector kit for effective light coupling in optical prototyping," *Optik* **201**, 163350 (2020).
50. M. Schmid, D. Ludescher, and H. Giessen, "Optical properties of photoresists for femtosecond 3D printing: refractive index, extinction, luminescence-dose dependence, aging, heat treatment and comparison between 1-photon and 2-photon exposure," *Opt. Mater. Express* **9**(12), 4564–4577 (2019).

51. R. Zvagelsky, D. Chubich, D. Kolymagin, E. Korostylev, V. Kovalyuk, A. Prokhodtsov, A. Tarasov, G. Goltsman, and A. Vitukhnovsky, "Three-dimensional polymer wire bonds on chip: morphology and functionality," *J. Phys. D: Appl. Phys.* **53**(35), 355102 (2020).
52. A. Žukauskas, G. Batavičiūtė, M. Ščiuka, T. Jukna, A. Melninkaitis, and M. Malinauskas, "Characterization of photopolymers used in laser 3D micro/nanolithography by means of laser-induced damage threshold (LIDT)," *Opt. Mater. Express* **4**(8), 1601–1616 (2014).
53. "The Institute of Electronic Structure and Laser of the Foundation for Research and Technology-Hellas (IESL-FORTH), Nonlinear Lithography group," https://www.iesl.forth.gr/en/research/NLL_Group.
54. E. Stankevičius, M. Malinauskas, and G. Račiukaitis, "Fabrication of scaffolds and micro-lenses array in a negative photopolymer SZ2080 by multi-photon polymerization and four-femtosecond-beam interference," *Phys. Procedia* **12**, 82–88 (2011).
55. A. Žukauskas, G. Batavičiūtė, M. Ščiuka, Z. Balevičius, A. Melninkaitis, and M. Malinauskas, "Effect of the photoinitiator presence and exposure conditions on laser-induced damage threshold of ORMOSIL(SZ2080)," *Opt. Mater.* **39**, 224–231 (2015).
56. J. Li, B. Jia, and M. Gu, "Engineering stop gaps of inorganic-organic polymeric 3D woodpile photonic crystals with post-thermal treatment," *Opt. Express* **16**(24), 20073–20080 (2008).
57. V. Kalima, I. Vartiainen, T. Saastamoinen, M. Suvanto, M. Kuitinen, and T. T. Pakkanen, "UV-curable ZnS/polymer nanocomposite for replication of micron and submicron features," *Opt. Mater.* **31**(10), 1540–1546 (2009).
58. S. Burgess, X. Li, and J. Holland, "High spatial resolution energy dispersive X-ray spectrometry in the SEM and the detection of light elements including lithium," *Microscopy and Analysis* **6**, S8–S13 (2013).
59. S. Demuru, L. Nela, N. Marchack, S. J. Holmes, D. B. Farmer, G. S. Tulevski, Q. Lin, and H. Deligianni, "Scalable nanostructured carbon electrode arrays for enhanced dopamine detection," *ACS Sens.* **3**(4), 799–805 (2018).
60. M. Lapine, I. V. Shadrivov, D. A. Powell, and Y. S. Kivshar, "Magnetoelastic metamaterials," *Nat. Mater.* **11**(1), 30–33 (2012).